Frontiers of Information Technology & Electronic Engineering
www.zju.edu.cn/jzus; engineering.cae.cn; www.springerlink.com
ISSN 2095-9184 (print); ISSN 2095-9230 (online)
E-mail: jzus@zju.edu.cn

Electrical analysis of single-walled carbon nanotube as gigahertz on-chip interconnects

Zamshed Iqbal CHOWDHURY[†‡1], Md. Istiaque RAHAMAN[2], M. Shamim KAISER[†1]

([1]*Institute of Information Technology, Jahangirnagar University, Dhaka 1342, Bangladesh*)

([2]*Department of Electrical & Electronic Engineering, Ahsanullah University of Science & Technology, Dhaka 1208, Bangladesh*)

[†]E-mail: zic@juniv.edu; mskaiser@juniv.edu

Received Oct. 21, 2015; Revision accepted Feb. 16, 2016; Crosschecked Dec. 23, 2016

Abstract: The single-walled carbon nanotube (SWCNT) is a promising nanostructure in the design of future high-frequency system-on-chip, especially in network-on-chip, where the quality of communication between intellectual property (IP) modules is a major concern. Shrinking dimensions of circuits and systems have restricted the use of high-frequency signal characteristics for frequencies up to 1000 GHz. Four key electrical parameters, impedance, propagation constant, current density, and signal delay time, which are crucial in the design of a high-quality interconnect, are derived for different structural configurations of SWCNT. Each of these parameters exhibits strong dependence on the frequency range over which the interconnect is designed to operate, as well as on the configuration of SWCNT. The novelty of the proposed model for solving next-generation high-speed integrated circuit (IC) interconnect challenges is illustrated, compared with existing theoretical and experimental results in the literature.

Key words: Interconnect; Carbon nanotube; Current density; Propagation constant; Characteristic impedance; System-on-chip

http://dx.doi.org/10.1631/FITEE.1500349 **CLC number:** TN402

1 Introduction

System-on-chip (SoC) and embedded computers are in extensive use all over the world today. Many of the necessary subsystems are available now for integration into a single chip to construct an SoC. These systems require less space and power, and can operate at very high frequencies. The astonishing development in semiconductor fabrication technologies in recent years has made it possible for more intellectual properties (IPs) and logic circuits being incorporated into a single chip. However, this development has led to a lot of engineering problems. With more logic circuits placed in a single chip, the performance requirements are facing steep challenges, most of which are architectural in nature. In specialized SoC architectures, where the communication between different IPs poses a great contribution towards the overall performance, such as network-on-chip (NoC), the challenge is to design the interconnects that meet the system requirements in terms of electrical performance. While the shrinking dimensions of modern integrated circuits and systems have reached the regime of nanometers, an inherent drawback is imposed on the appropriate interconnect material. This would cause negligible decline in electrical performance, and meanwhile allow a higher scale of integration. As interconnects in a chip are reducing in their dimensions, the problem due to the characteristic behavior of the interconnect material is contributing to design constraints. The

‡ Corresponding author
ORCID: Zamshed Iqbal CHOWDHURY, http://orcid.org/0000-0002-4096-7000

©Zhejiang University and Springer-Verlag Berlin Heidelberg 2017

quality of an interconnect is based on several factors, including signal propagation delay, power consumption, and electrical behavior at lower dimensions. For a high-frequency SoC, it is desirable that the interconnect network is fast enough to maintain synchronized operations throughout the chip. As the most widely used material presently, copper faces two fundamental and critical problems: its incapability of providing high current density, and the augmented electrical resistivity at reduced dimensions. In terms of electrical resistivity, the enhancement is due to surface scattering of electrons, and the problems due to grain boundaries (Zhou *et al.*, 2008). In the sub-100-nm region, copper suffers from a considerable wire delay. According to the International Technology Roadmap for Semiconductors (ITRS), the resistivity of copper will jump from 40.8 to 81.9 Ω·nm for both dimensions of 45 and 14 nm, causing severe degradation in the performance (Allan *et al.*, 2002). In low-power systems, this would cause more power dissipation by the interconnect network itself. The delay in a global interconnection network will cause signals to take multiple clock cycles to cross the entire chip, thereby degrading the NoC performance. The single-walled carbon nanotube (SWCNT) has shown promise as a solution to these problems. First, the resistance of the carbon nanotube is smaller than that of copper wires for dimensions below 60 nm. Second, CNT has a larger mean free path (∼1 μm) at room temperature, as compared to copper (∼40 nm) in bulk material (Zhou *et al.*, 2008). If the mean free path is greater than the length of the interconnect link, electrons will exhibit a ballistic transport phenomenon while traversing the nanotube. Unlike copper, where electromigration plays a significant role in determining the performance of interconnects, CNT would experience less of this phenomenon (Galand *et al.*, 2013). Furthermore, CNTs could be treated to have fewer particles on their inner walls (Baughman *et al.*, 2002; Yuzvinsky *et al.*, 2006).

Electrical modeling of SWCNTs has been in the minds of researchers for quite some time now. The probability of using SWCNTs in nanometer very-large-scale integration (VLSI) applications has been evaluated in terms of the time delay and power consumed at 22 and 14 nm dimensions with the help of capacitance modeling of an SWCNT bundle and the associated inductive effects (Srivastava *et al.*, 2009). Nieuwoudt and Massoud (2006) evaluated the SWCNT bundle using magnetic inductance modeling techniques (Nieuwoudt and Massoud, 2006). Although much previous work has theorized, examined, and discussed the electrical parameters, such as frequency-dependent impedance (Burke, 2002a), delay time in CNT bundle interconnects (Srivastava and Banarjee, 2005; Srivastava *et al.*, 2009), and variations in AC and DC conductivities (Ounaies *et al.*, 2003), it has not evaluated the relevant electrical parameters, which are also vital in determining CNT's suitability in VLSI applications, such as the attenuation constant and the importance of impedance matching between contact resistance and characteristic impedance of SWCNT. Furthermore, the mentioned parameters have not been evaluated in terms of their dependence on the signal frequency or structural parameters. Since the electrical behavior depends on the nanotube diameter as well, a framework is required to determine the best suited configuration for a particular application.

We evaluate the possibility of using isolated SWCNT interconnects for high-frequency VLSI applications. The detailed derivations of necessary SWCNT parameters, considering their frequency-dependent characteristics and structural parameters, are presented. The major electrical parameters of interconnects, namely the impedance, propagation constant, current density, and signal delay time, are analyzed with emphasis on the frequency of the electrical signal. An isolated SWCNT is considered because of the reduced dimension and power requirements of interconnects, as well as the recent development in the growth of isolated SWCNTs with very small dimensions (Liu and Cheng, 2013; Fagan *et al.*, 2015). Since the Fermi liquid model breaks down in one dimension, the Lüttinger liquid theory is used for the determination of gigahertz (GHz) electrical properties of SWCNT, which assumes that CNT behaves as a 1D plasmon. A few optimization possibilities in interconnect systems are also discussed and analyzed, considering the simulated behavior.

2 Carbon nanotube structure and theoretical models

A graphene sheet that is rolled up to form a seamless tube-like structure eventually forms SWCNT. The electrical properties of SWCNT have a strong dependence on the chirality and the nan-

otube diameter. The electrical behavior of SWCNT can be easily altered by varying a pair of structural indices (n, m), which denotes the number of unit vectors along two directions in the honeycomb crystal lattice of graphene.

SWCNTs can be produced in a number of ways, such as by laser vaporization of a graphite rod doped with Co and Ni (Thess *et al.*, 1996), and by arc evaporation of a graphite rod doped with Y and Ni (Journet *et al.*, 1997). For the controlled growth of SWCNT, the dependence of electrical properties on the indices (n, m) can be used by varying the Co:Ni ratio in bimetallic Co−Ni−MCM 41 catalysts (Cursaru *et al.*, 2011).

Depending on the chirality and the indices (n, m), CNTs are divided into three major groups: armchair, zigzag, and spiral. The diameter d of SWCNT also depends only on (n, m) (Anantram and Léonard, 2006). In effect the domain of electrical behavior of the tube, either semiconducting or metallic, is chosen, and d can be expressed as

$$d=\frac{\sqrt{3}a}{2\pi}\sqrt{n^2+nm+m^2}, \tag{1}$$

where $a=0.142$ nm is the bond length between carbon atoms. Depending on the range of values m and n can take, SWCNTs are divided into three categories: zigzag CNTs ($m=0$), armchair CNTs ($n=m$), and chiral CNTs (otherwise).

SWCNT shows length-dependent specific resistivity, while copper and tungsten show no such dependence. This dependence illustrates an exponential behavior with a negative slope, and tends to reach a quasi-saturation level, as tube length increases up to 100 μm and beyond (Kreupl, 2008). The very large mean free path of the charge carriers in SWCNT contributes to this dependence. SWCNTs that exceed the limit of the mean free path have a significantly better resistance per unit length in comparison to copper, approximated to ∼6 kΩ/μm.

Earlier models describing CNT behavior are indifferent to the change in the frequency of the system. SWCNTs are considered as 1D conductors, in which strong coulomb interactions between electrons modify the properties away from conventional conductors considered as Fermi liquids. Burke (2002a) modeled the microwave properties of CNTs using the Lüttinger liquid theory. CNTs can be considered to act like a Lüttinger liquid, where the electrons interact with each other, thereby causing different electrical parameters to develop. Zhao *et al.* (2001) suggested that the electrical parameters of CNTs show a behavior that is very much dependent on the frequency.

3 Mathematical modeling

Depending on the spin-up or spin-down conditions, an isolated nanotube has four different propagation channels owing to its band structure. Following Burke (2002a), the circuit diagram shown in Fig. 1 can be considered as an effective circuit model for the charged mode transfer, where e is the Euler number, L_{K} is the kinetic inductance, C_{Q} and C_{ES} are the quantum and electrostatic capacitances, respectively.

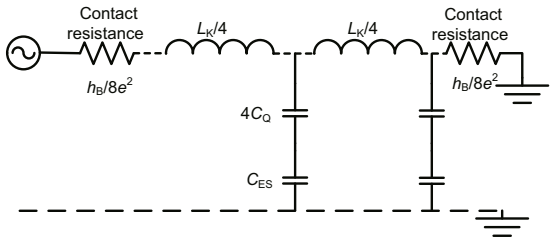

Fig. 1 Equivalent circuit diagram of an single-walled carbon nanotube with DC electrical contacts at both ends

3.1 Nanotube impedance (Z_{Nanotube})

Neglecting the damping mechanism caused by the ground plane, the impedance of a nanotube can be written as (Burke, 2002b)

$$Z_{\mathrm{Nanotube}}=\frac{h_{\mathrm{B}}}{8e^2}+\frac{R_{\mathrm{C}}}{2}+Z_{\mathrm{c,effective}}.\frac{1+\Gamma \mathrm{e}^{-2\gamma l}}{1-\Gamma \mathrm{e}^{-2\gamma l}}, \tag{2}$$

where $Z_{\mathrm{c,effective}}$ is the characteristic impedance of the nanotube, h_{B} is Planck's constant, Γ is the reflection coefficient, l is the total length of the nanotube, R_{C} is the resistance due to imperfect contact, and γ is the propagation constant of a 1D plasmon. γ, Γ, and $Z_{\mathrm{c,effective}}$ are expressed as (Burke, 2002a; McEuen *et al.*, 2002)

$$\gamma\equiv\sqrt{(R+\mathrm{i}\omega L_{\mathrm{eff}})\,\mathrm{i}\omega C_{\mathrm{eff}}}, \tag{3}$$

$$\Gamma=\frac{Z_{\mathrm{L}}-Z_{\mathrm{c,effective}}}{Z_{\mathrm{L}}+Z_{\mathrm{c,effective}}}, \tag{4}$$

$$Z_{\mathrm{c,effective}}\approx\sqrt{\frac{R+\mathrm{i}\omega L_{\mathrm{eff}}}{\mathrm{i}\omega C_{\mathrm{eff}}}}, \tag{5}$$

where R is the distributed resistance, ω is the angular frequency, Z_{L} is the contact resistance, and L_{eff} and C_{eff} are the effective inductance and capacitance, respectively. R_{C} has an additive effect on the load impedance in case of an imperfect contact. If Γ becomes zero, Eq. (2) reduces to

$$Z_{\mathrm{Nanotube}} = \frac{h_{\mathrm{B}}}{8e^2} + \frac{R_{\mathrm{C}}}{2} + Z_{\mathrm{c,effective}}, \tag{6}$$

which approximates the tube impedance to be independent of the 1D plasmon propagation constant. From the equivalent circuit of Fig. 1, it can be seen that (Ismail *et al.*, 2000; Burke, 2002b)

$$\begin{aligned} L_{\mathrm{eff}} &\cong \frac{L_{\mathrm{K}}}{4} \cdot f^{-0.87} \cong \frac{h_{\mathrm{B}}}{8e^2 v_{\mathrm{F}}} \cdot f^{-0.87} \\ &\approx 4f^{-0.87} \ \ \mathrm{nH/\mu m}, \end{aligned}$$

$$\frac{C_{\mathrm{eff}}}{f^{-0.87}} \cong \left(4{C_{\mathrm{Q}}}^{-1} + {C_{\mathrm{ES}}}^{-1}\right)^{-1} = \frac{2\pi\epsilon}{\dfrac{2h_{\mathrm{B}}v_{\mathrm{F}}}{e^2} + \ln\dfrac{h}{d}},$$

where $v_{\mathrm{F}} = 8 \times 10^5$/ms is the Fermi velocity, and ϵ is the permittivity. Since a 1D plasmon wave decays along the length of the nanotube, the decay length l_{decay} is approximated to be at least as long as the mean free path of CNT (Burke, 2002a):

$$l_{\mathrm{decay}} = \frac{2Z_{\mathrm{c,effective}}}{R}. \tag{7}$$

Substituting the value of R from the above expression into Eq. (5) yields

$$Z_{\mathrm{c,effective}} = \left[\frac{2\dfrac{Z_{\mathrm{c,effective}}}{l_{\mathrm{m.f.p.}}} + \mathrm{i}\omega\dfrac{h_{\mathrm{B}}}{8e^2v_{\mathrm{F}}} \cdot f^{-0.87}}{\mathrm{i}\omega\left(\dfrac{2h_{\mathrm{B}}v_F}{e^2} + \dfrac{\ln(h/d)}{2\pi\epsilon}\right)^{-1} \cdot f^{-0.87}}\right]^{\frac{1}{2}}, \tag{8}$$

where 'm.f.p' denotes free path length. Eq. (8) is a quadratic equation of the form

$$\begin{aligned} &{Z_{\mathrm{c,effective}}}^2 \cdot \mathrm{i}\omega\left(\frac{2h_{\mathrm{B}}v_{\mathrm{F}}}{e^2} + \frac{\ln(h/d)}{2\pi\epsilon}\right)^{-1} \cdot f^{-0.87} \\ &-\frac{2Z_{\mathrm{c,effective}}}{l_{\mathrm{m.f.p.}}} - \mathrm{i}\omega \cdot \frac{h_{\mathrm{B}}}{8e^2v_{\mathrm{F}}} \cdot f^{-0.87} = 0, \end{aligned} \tag{9}$$

which has the following solutions:

$$\begin{aligned} Z_{\mathrm{c,effective}} = \frac{1}{4\chi e^2}\Big[&2\times10^6 \\ &\pm\sqrt{4\times10^{12} - \chi\omega^2 h_{\mathrm{B}} f^{-0.87}}\Big], \end{aligned} \tag{10}$$

where $\chi = \pi\epsilon\left(4h_{\mathrm{B}}v_{\mathrm{F}}\pi\epsilon + \ln(h/d)\,e^2\right)^{-1} \cdot f^{-0.87}$. From Eqs. (6) and (10), the impedance of the nanotube can be calculated by assuming a perfect contact ($R_{\mathrm{C}} = 0$) and a perfectly matched load. Now, using the high-frequency limit as stated in Eq. (2) (Burke, 2002a), and assuming a perfect contact, Z_{Nanotube} can be expressed as

$$Z_{\mathrm{Nanotube}} = \frac{h_{\mathrm{B}}}{8e^2}\left(1 + \frac{1}{g} \cdot \frac{1 + \Gamma\mathrm{e}^{-2\frac{2\pi}{\lambda}l}}{1 - \Gamma\mathrm{e}^{-2\frac{2\pi}{\lambda}l}}\right), \tag{11}$$

where the value of γ is considered using the high-frequency limit, expressed as

$$\lim_{\omega\to R/L_{\mathrm{eff}}} \gamma = k \equiv \frac{2\pi}{\lambda} = \frac{\omega}{v_{\mathrm{p}}}. \tag{12}$$

In the extreme condition,

$$\lim_{\Gamma\to0} Z_{\mathrm{Nanotube}} = \frac{h_{\mathrm{B}}}{8e^2}\left(1 + \frac{1}{g}\right), \tag{13}$$

where g is the Lüttinger constant, which defines the coulomb interaction among electrons, and v_{p} is the phase velosity. It is clear that Z_{Nanotube} becomes independent of the total length, as the impedance of the load approaches the value of the characteristic impedance of the tube. Since the load reflects no portion of the forward wave, Z_{Nanotube} will approach its quantum limit for a definite value of g.

3.2 Attenuation and phase delay constant

Parameter γ is the amalgamation of the attenuation constant and phase constant of a signal. Attenuation constant α, which is the real part of complex entity γ, defines the rate at which the fields of the propagating wave are attenuated. Using Eq. (3) and equating the real and imaginary parts yields

$$\alpha^2 - \beta^2 = -\omega^2 L_{\mathrm{eff}} C_{\mathrm{eff}}, \tag{14}$$

$$2\alpha\beta = -\omega R C_{\mathrm{eff}}, \tag{15}$$

where β is the phase delay constant. Solving β and substituting it into Eq. (14) yields

$$A^2 - 4\omega^2 L_{\mathrm{eff}} C_{\mathrm{eff}} A - \omega^2 R^2 {C_{\mathrm{eff}}}^2 = 0, \tag{16}$$

where $A = \alpha^2$. Eq. (16) is a quadratic equation and has the following solutions:

$$\alpha = \sqrt{2\omega C_{\mathrm{eff}}\left(-\omega L_{\mathrm{eff}} \pm \sqrt{4{L_{\mathrm{eff}}}^2 - R^2}\right)}. \tag{17}$$

The solution with the negative sign gives a value of α that is not real. Thus, the solution with the positive sign is the only valid root. Similarly, the expression for β is derived from Eqs. (15) and (17) as

$$\beta = R^2 \left[\frac{\omega C_{\text{eff}}}{8\left(-\omega L_{\text{eff}} \pm \sqrt{4{L_{\text{eff}}}^2 - R^2}\right)} \right]^{\frac{1}{2}}. \quad (18)$$

3.3 Current density (J_{CNT}) and transient response

Current density and power spectral density are very important parameters for any interconnect. Considering only a single section per unit length, the equivalent circuit of an SWCNT is essentially an RLC circuit (Fig. 2), from which the system equation can be written as

$$u(t) = Ri_{\text{T}} + L_{\text{eff}} \cdot \frac{\mathrm{d}i_{\text{T}}}{\mathrm{d}t} + V_{\text{C}}(t), \quad (19)$$

where $V_{\text{C}}(t)$ is the time-dependent voltage developed across the capacitive elements, and i_{T} is the total current. $V_{\text{C}}(t)$ interprets the change in voltage along the length of the nanotube. Using the equation of the current through a capacitive element, Eq. (19) takes the following differential form:

$$u(t) = L_{\text{eff}}C_{\text{eff}} \cdot \frac{\mathrm{d}^2V_{\text{C}}}{\mathrm{d}t^2} + RC_{\text{eff}} \cdot \frac{\mathrm{d}V_{\text{C}}}{\mathrm{d}t} + V_{\text{C}}(t), \quad (20)$$

which has the following solution:

$$V_{\text{C}}(t) = K_1\exp(-s_1t) + K_2\exp(-s_2t) + u(t) \cdot f,$$

where

$$s = \left(-RC_{\text{eff}} \pm \sqrt{(RC_{\text{eff}})^2 - 4L_{\text{eff}}C_{\text{eff}}}\right)(2L_{\text{eff}}C_{\text{eff}})^{-1},$$

and K_1 and K_2 are the natural and forced response constants, respectively, which have the following forms:

$$K_1 = -f\left[-u(0) + \left(s_1u(0) + \left.\frac{\mathrm{d}u(t)}{\mathrm{d}t}\right|_{t=0}\right) \cdot \frac{1}{s_2 - s_1}\right],$$

$$K_2 = f\left(s_1u(0) + \left.\frac{\mathrm{d}u(t)}{\mathrm{d}t}\right|_{t=0}\right) \cdot \frac{1}{s_2 - s_1}.$$

Now, $i_{\text{T}} = i_{\text{L}} = i_{\text{C}} = C_{\text{eff}} \cdot \dfrac{\mathrm{d}V_{\text{C}}}{\mathrm{d}t}$. Thus, we have

$$\begin{aligned} i_{\text{T}} = C_{\text{eff}}f &\left(-u(0) + \frac{s_1u(0) + \left.\dfrac{\mathrm{d}u(t)}{\mathrm{d}t}\right|_{t=0}}{s_2 - s_1}\right) \\ &\cdot\exp(-s_1t) \cdot s_1 - f \cdot \frac{s_1u(0) + \left.\dfrac{\mathrm{d}u(t)}{\mathrm{d}t}\right|_{t=0}}{s_2 - s_1} \\ &\cdot\exp(-s_2t) \cdot s_2 + f \cdot \frac{\mathrm{d}u(t)}{\mathrm{d}t}, \end{aligned} \quad (21)$$

and the current through the output branch is

$$i_0(t) = \frac{V_{\text{C}}(t)}{R_{\text{OC}}} = \frac{V_{\text{C}}(t)}{R_{\text{L}}}, \quad (22)$$

where R_{OC} is the open circuit resistance, and R_{L} is the load resistance. Thus, the current density is

$$J_{\text{CNT}} = \frac{i_{\text{T}}\pi}{3a^2\left(n^2 + nm + m^2\right)}.$$

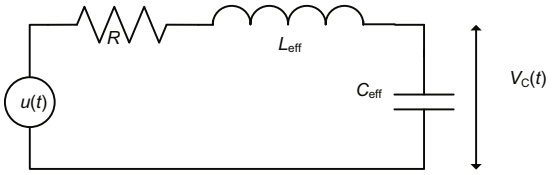

Fig. 2 Equivalent electrical circuit diagram of single-walled carbon nanotube

3.4 Signal delay (S_{W})

Signal delay is evaluated in terms of 50% delay and rise times of the signals through SWCNT. To estimate the signal delay caused by a particular SWCNT configuration, the equivalent Elmore delay approximation for RLC trees is used (Ismail *et al.*, 2000). Although the Elmore approximation considers only the effect of resistance and the capacitance of a section, the effect of inductance is considered as well. The single RLC section of a nanotube has a transfer function

$$g(s) = \left(s^2R_{\text{eff}}C_{\text{eff}} + sL_{\text{eff}}C_{\text{eff}} + 1\right)^{-1}, \quad (23)$$

where R_{eff} is the effective resistance including contact resistance. Rearranging the above expression yields

$$g(s) = \frac{{\omega_n}^2}{s^2 + 2s\omega_n\xi + {\omega_n}^2}, \quad (24)$$

where $\xi = \dfrac{R_{\text{eff}}C_{\text{eff}}}{2\sqrt{L_{\text{eff}}C_{\text{eff}}}}$ is the damping factor of the system, and $\omega_n = (L_{\text{eff}}C_{\text{eff}})^{-1/2}$. The system poles are $\text{Pole}_{1,2} = \omega_n\left(-\xi \pm \sqrt{\xi^2-1}\right)$. Depending on the value of ξ, three scenarios are possible: underdamped ($\xi < 1$), overdamped ($\xi > 1$), and critically damped ($\xi = 1$) responses. It has already been proven by Ismail *et al.* (2000) that kinetic inductance (L_{K}) dominates over magnetic inductance (L_{M}). Thus, the response should be monotonic as long as ξ stays less than unity. According to Ismail *et al.* (2000), 50% delay (t_{pdi}) and the rise times (t_{ri}) are derived as

$$t_{\text{pdi}} = \frac{1}{\omega_{\text{ni}}}1.047\exp\left(-\frac{\xi_i}{0.85}\right) + 0.695R_{\text{eff}}C_{\text{eff}}, \quad (25)$$

$$t_{\text{ri}} = \frac{1}{\omega_{\text{ni}}}\left(6.017\exp\left(-\frac{{\xi_i}^{1.35}}{0.4}\right) - 5\exp\left(-\frac{{\xi_i}^{1.25}}{0.64}\right)\right) + 2.195R_{\text{eff}}C_{\text{eff}}. \quad (26)$$

For a square wave, the rise time, pulse width, and fall time should be the same. Therefore, it is assumed that $t_{\text{ri}} = t_{\text{f}} = t_{\text{f}}$, where t_{f} is the 50% fall time and t_{f} is the width of the pulse. Thus, the total time period should be $T = 3t_{\text{ri}}$, and the maximum frequency component must be less than $(3t_{\text{ri}})^{-1}$. However, as CNT possesses the exceptional property of frequency-dependent impedance, this maximum frequency limit or bandwidth should depend on the fundamental frequency as well.

4 Simulation results and analyses

The technology node information used in simulations is taken from Allan *et al.* (2002). The equations derived from the mathematical model are simulated at 18 nm node and analyzed. Fig. 3 illustrates the variation of characteristic impedance as the frequency increases toward the terahertz (THz) region. The characteristic impedance shows a rise in magnitude as the frequency increases. The pattern of rise should be quasi-linear in nature with a perfect impedance matching. The experimentally found nanotube impedance conforms to this behavior up to 5 GHz (Iqbal *et al.*, 2014).

From Fig. 4, it is evident that Z_{Nanotube} depends only on g for all values of l when an impedance-matching network is considered. The range of g ensures the long-range columbic interactions among

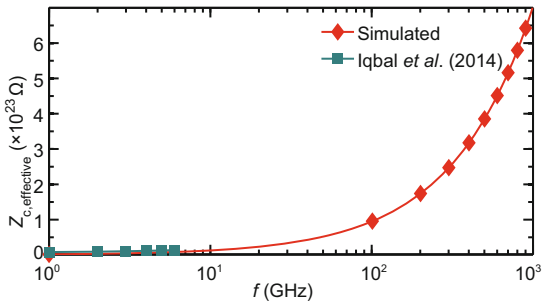

Fig. 3 Characteristic impedance versus the frequency of operation

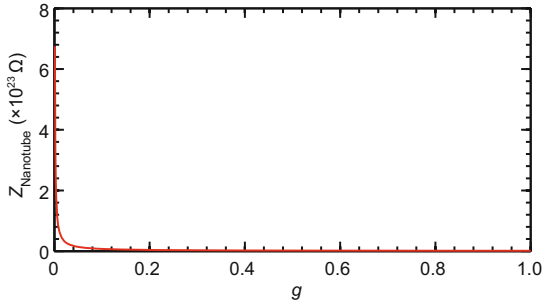

Fig. 4 Projected Z_{Nanotube} as Lüttinger constant g varies

electrons in SWCNT (Kane *et al.*, 1997). The fact that g actually determines the degree of interaction between electrons propagating through the nanotube suggests that if a perfect impedance-matching network is used at both ends, the tube impedance would be constant for a given length of the tube, while g remains constant. However, a matching network which could provide a perfect matching of impedance is unlikely to be achieved. Thus, assuming an imperfect contact and a matching network would yield the trend of Z_{Nanotube}, which is dependent on the length of tube in a nearly exponential manner. Note that an imperfect contact could lead to a nonzero Γ, which is actually responsible for the variations in Z_{Nanotube} at different lengths. There is currently no experimental result illustrating the dependence of Z_{Nanotube} on the varying degrees of g.

The amount of power to be transmitted over a tube length before detection of the signal is directly dependent on α. It can be seen from Fig. 5 that α varies with the signal frequency in an incremental manner. α changes quite abruptly and linearly toward higher values at lower frequencies, which lasts up to 100 GHz, in accordance with the experimental findings presented by Dragoman *et al.* (2006). However, as the frequency increases toward higher values, α tends to get saturated, as shown by a decreasing

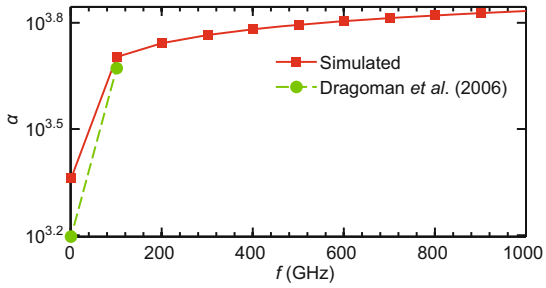

Fig. 5 Expected trend of the attenuation constant α with frequency f up to 1 THz

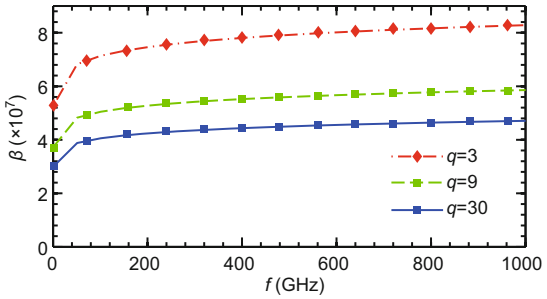

Fig. 6 Expected trend of the phase constant β with frequency f up to 1 THz and q=3, 9, and 30

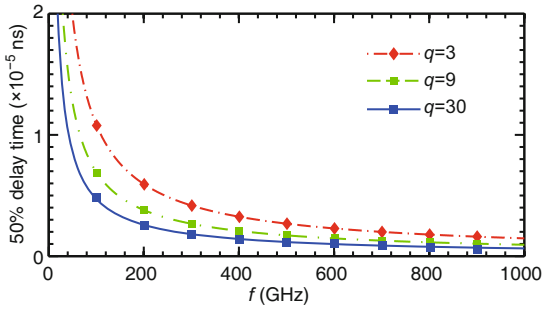

Fig. 7 Expected trend of 50% delay time with frequency f up to 1 THz and q=3, 9, and 30

slope. Beyond the THz (1 THz = 1000 GHz) regime, α should attain a quasi-saturation state.

The pattern demonstrated by β is quite similar to that expected in the case of α. The only difference is that the pattern is exponential in nature with a declining slope as the frequency approaches 1 THz. As the frequency of operation extends into THz region, β tends to settle to saturated or quasi-saturated values. Fig. 6 illustrates the projected value of β with an increasing frequency of operation. The structural ratio q, which is the ratio of the height of the nanotube from the ground plane (h) and diameter of the tube (d), is varied between 3 and 30. It is predicted that as the frequency increases, the value of β depends largely on how this ratio is set. This is another distinction compared to α, as there is no change in the pattern demonstrated by α with varying values of q. Although Jespersen and Nygård (2005) presented the phase shift in CNT with experimental validation, there are no scientific data on the determination of the phase constant of a wave traversing through an SWCNT.

Fig. 7 illustrates the simulated behavior of 50% delay time for frequencies ranging up to 1 THz. The behavior is expected to be semi-exponential in nature, with a drastic drop in the delay time within the first quarter of the 100 GHz region. This delay time is also sensitive to q, as can be observed from the figure. The delay time is expected to fall as q varies from its initial value of 3 to 9 and 30. The frequencies above 300 GHz experience negligible delay in decreasing order as they approach the THz region. The length dependence of the 50% delay time has been reported in the literature (Liang *et al.*, 2011); however, the frequency-dependent behavior of the delay time has not been found.

The parameter t_{ri} is an indication of how well a step signal can be conducted through a medium, which is an attribute necessary for any interconnect in digital and mixed signal VLSI systems. The less the time it takes to rise to 50% of its final value, the better and faster the interconnect. Fig. 8 illustrates the anticipated behavior of t_{ri} up to the THz region. It can be observed that beyond 400 GHz, t_{ri} tends to settle down to a very low value (very close to 0.1 in the linear scale). In the lower frequency region (0–200 GHz), t_{ri} shows an exponential behavior with a longer time to rise to 50% of the final value. Fig. 8 also shows an interesting structural dependence of t_{ri} on the ratio q. t_{ri} is inclined to have an oscillating characteristic in the 0–200 GHz region, with the maximum values decreasing and increasing as q is increased. Although experimental data on the variation in rise time with variation in the concentration

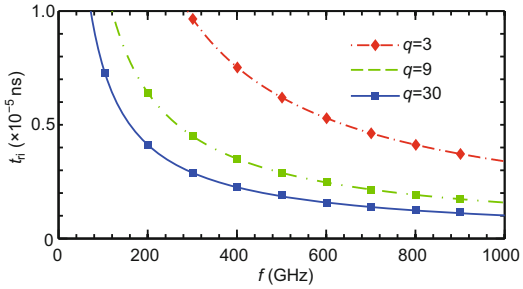

Fig. 8 Simulated behavior of 50% rise time t_{ri} with frequency up to 1 THz and q=3, 9, and 30

of CNT were provided by Huang *et al.* (2005), there has been no significant research on the determination of the frequency dependence of the signal rise time.

According to the model developed, J_{CNT} in SWNCT depends on two parameters, q and d. Figs. 9a–9e show that J_{CNT} (A/cm^2) highly depends on the structural parameters of CNT (n, m). Figs. 9a–9c show that J_{CNT} varies over a significant extent while n and m are varied to produce zigzag, armchair, and chiral nanotubes. J_{CNT} is maximum in the armchair structure, while chiral structure tends to have the lowest J_{CNT}. In comparison to the experimental findings in the literature, which reports a current density of 2×10^6 A/cm^2 through vertical MWCNT vias (Nihei *et al.*, 2004), the current density in different configurations of SWCNT shows a promise to attain a close level of current density with a 1 THz signal. J_{CNT} also demonstrates a substantial dependence on q. This trend is illustrated in Figs. 9d and 9e for a nanotube having an armchair configuration. When q is increased, the trend seems to attain a parabolic behavior. The expected value of J_{CNT} in such configurations can equal the experimental findings available in the literature with 1 THz signals (McEuen *et al.*, 2002). The illustrated experimental current densities are constant since only the maximum current densities are reported. The simulated SWCNT interconnect parameters are listed in Table 1 with the respective dependence and limitations. This table can be used as a design framework for SWCNT interconnects for specific applications or systems.

5 Conclusions

An isolated SWCNT is modeled and simulated with different structural configurations in terms of four key electrical parameters, namely nanotube impedance, attenuation and phase delay constants, current density, and signal delays, which are critically important for designing high-performance VLSI interconnects. The simulation outcomes are compared with available research findings. It is shown that while SWCNT holds promise and opportunities for the design of future nano-interconnect networks, it needs careful evaluation before being implemented in a particular design process. For instance, to neglect the effect of the propagation constant on nanotube impedance, the characteristic impedance of

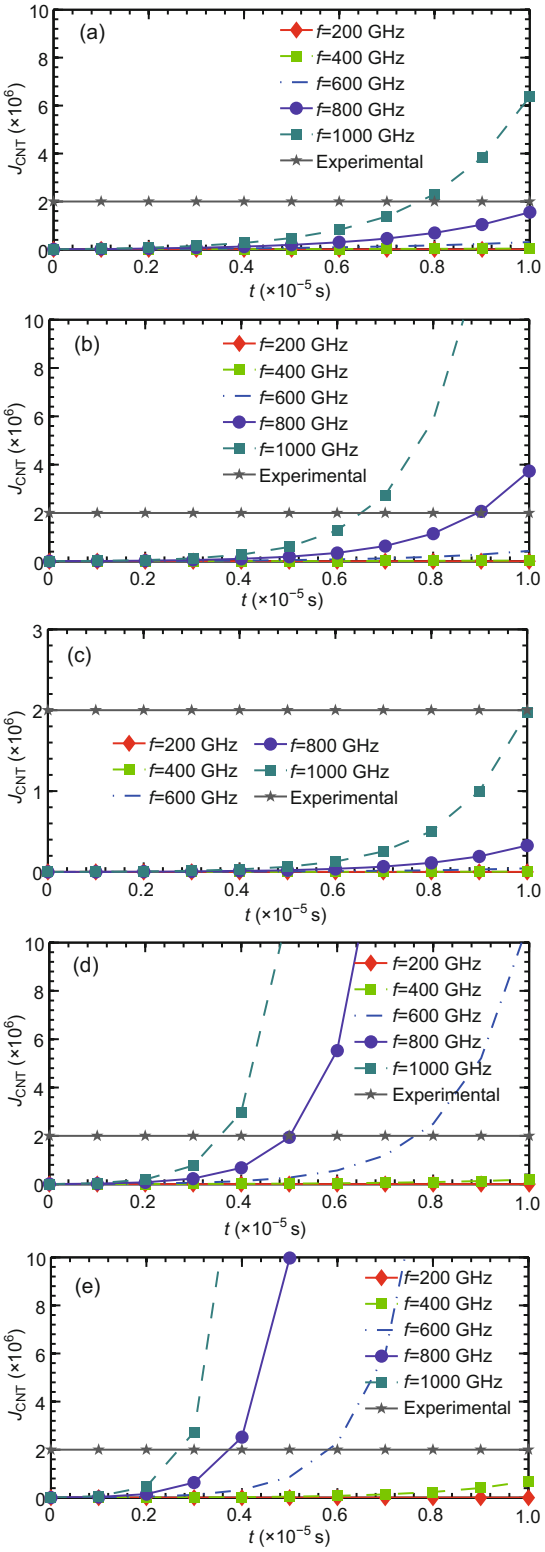

Fig. 9 Current density in different types of single-walled carbon nanotube: (a) a zigzag SWCNT (m=0, n=1, q=3); (b) an armchair SWCNT (m=1, n=1, q=3); (c) a chiral SWCNT (m=3, n=2, q=3); (d) an armchair SWCNT (m=1, n =1, q=9); (e) an armchair SWCNT (m=1, n=1, q=30)

Table 1 Summary of simulated system parameters

Electrical parameter	Nature of variation	Dependence	Dependence on parameter	Limiting value
$Z_{\mathrm{c,Nanotube}}$	Quasi-linear	No	–	8×10^{23} Ω
Z_{Nanotube}	Exponential	Yes	g	Very close to zero
α	Linear initially, then tending to saturate	Yes	–	Quasi-saturated value
β	Exponential	Yes	f, t	–
50% delay	Exponential	Yes	q, f	Very close to zero
t_{ri}	Exponential	Yes	q, f	Very close to zero
J_{CNT}	Increased slope with increasing frequency	Yes	n, m, d, q	–

the nanotube and the terminal resistance should be closely matched for reduced reflection, thereby enabling efficient transfer of energy throughout the nanotube, which is essential for designing a low-power interconnect. From the detailed mathematical model and analysis of the anticipated behavior of the concerned signal and structural parameters, it was shown that there is a direct correlation between the nanotube structural configuration and other electrical and signal properties. This work provides insight into these issues while presenting a rough approximation to a framework, which is necessary for the design of high-frequency VLSI interconnect networks.

References

Allan, A., Edenfeld, D., Joyner, W.H., *et al.*, 2002. 2001 technology roadmap for semiconductors. *Computer*, **35**(1):42-53. http://dx.doi.org/10.1109/2.976918

Anantram, M.P., Léonard, F., 2006. Physics of carbon nanotube electronic devices. *Rep. Prog. Phys.*, **69**(3):507-561. http://dx.doi.org/10.1088/0034-4885/69/3/R01

Baughman, R.H., Zakhidov, A.A., de Heer, W.A., 2002. Carbon nanotubes—the route toward applications. *Science*, **297**(5582):787-792. http://dx.doi.org/10.1126/science.1060928

Burke, P.J., 2002a. Lüttinger liquid theory as a model of the gigahertz electrical properties of carbon nanotubes. *IEEE Trans. Nanotechnol.*, **1**(3):129-144. http://dx.doi.org/10.1109/TNANO.2002.806823

Burke, P.J., 2002b. An RF circuit model for carbon nanotubes. Proc. 2nd IEEE Conf. on Nanotechnology, p.393-396. http://dx.doi.org/10.1109/NANO.2002.1032273

Cursaru, D., Enescu, D., Ciuparu, D., 2011. Control of (n, m) selectivity in single wall carbon nanotubes (SWNT) growth by varying the Co-Ni ratio in bi-metallic Co-Ni-MCM 41 catalysts. *Rev. Chim.-Bucharest*, **62**(7):792-798.

Dragoman, M., Grenier, K., Dubuc, D., *et al.*, 2006. Experimental determination of microwave attenuation and electrical permittivity of double-walled carbon nanotubes. *Appl. Phys. Lett.*, **8**(15):1-3. http://dx.doi.org/10.1063/1.2193464

Fagan, A.J., Hároz, E.H., Ihly, R., *et al.*, 2015. Isolation of >1 nm diameter single-wall carbon nanotube species using aqueous two-phase extraction. *ACS Nano*, **9**(5):5377-5390. http://dx.doi.org/10.1021/acsnano.5b01123

Galand, R., Brunetti, G., Arnaud, L., *et al.*, 2013. Microstructural void environment characterization by electron imaging in 45 nm technology node to link electromigration and Copper microstructure. *Microelectron. Eng.*, **106**:168-171. http://dx.doi.org/10.1016/j.mee.2013.01.018

Huang, C.Y., Hu, C.Y., Pan, H.C., *et al.*, 2005. Electrooptical responses of carbon nanotube-doped liquid crystal devices. *Jpn. J. Appl. Phys.*, **44**(11):8077-8081. http://dx.doi.org/10.1143/JJAP.44.8077

Iqbal, M.Z., Puigdemont, J.P., Eom, J., *et al.*, 2014. High-frequency impedance of single-walled carbon nanotube networks on transparent flexible substrate. *Phys. Status Sol. B*, **251**(12):2461-2465. http://dx.doi.org/10.1002/pssb.201451233

Ismail, Y., Friedman, E.G., Neves, J.L., 2000. Equivalent Elmore delay for RLC trees. *IEEE Trans. Comput.-Aided Des. Integr. Circ. Syst.*, **19**(1):83-97. http://dx.doi.org/10.1109/43.822622

Jespersen, T.S., Nygård, J., 2005. Charge trapping in carbon nanotube loops demonstrated by electrostatic force microscopy. *Nano Lett.*, **5**(9):1838-1841. http://dx.doi.org/10.1021/nl0505997

Journet, C., Maser, W.K., Bernier, P., *et al.*, 1997. Large-scale production of single-walled carbon nanotubes by the electric-arc technique. *Nature*, **388**(6644):756-758. http://dx.doi.org/10.1038/41972

Kane, C., Balents, L., Fisher, M.P., 1997. Coulomb interactions and mesoscopic effects in carbon nanotubes. *Phys. Rev. Lett.*, **79**(25):5086-5089. http://dx.doi.org/10.1103/PhysRevLett.79.5086

Kreupl, F., 2008. Carbon nanotubes in microelectronic applications. *In*: Hierold, C., Brand, O., Fedder, G.K. (Eds.), Carbon Nanotube Devices: Properties, Modelling, Integration and Applications. Wiley-VCH Verlag GmbH & Co. KGaA, Weinheim, Germany, p.1-42. http://dx.doi.org/10.1002/9783527622597.ch1

Liang, F., Wang, G., Ding, W., 2011. Estimation of time delay and repeater insertion in multiwall carbon nanotube interconnects. *IEEE Trans. Electron. Dev.*, **58**(8):2712-2720. http://dx.doi.org/10.1109/TED.2011.2154334

Liu, C., Cheng, H.M., 2013. Carbon nanotubes: controlled growth and application. *Mater. Today*, **16**(1-2):19-28. http://dx.doi.org/10.1016/j.mattod.2013.01.019

McEuen, P.L., Fuhrer, M.S., Park, H., 2002. Single-walled carbon nanotube electronics. *IEEE Trans. Nanotechnol.*, **99**(1):78-85. http://dx.doi.org/10.1109/TNANO.2002.1005429

Nieuwoudt, A., Massoud, Y., 2006. Understanding the impact of inductance in carbon nanotube bundles for VLSI interconnect using scalable modeling techniques. *IEEE Trans. Nanotechnol.*, **5**(6):758-765. http://dx.doi.org/10.1109/TNANO.2006.883480

Nihei, M., Horibe, M., Kawabata, A., *et al.*, 2004. Carbon nanotube vias for future LSI interconnects. Proc. IEEE Int. Interconnect Technology Conf., p.251-253. http://dx.doi.org/10.1109/IITC.2004.1345767

Ounaies, Z., Park, C., Wise, K.E., *et al.*, 2003. Electrical properties of single wall carbon nanotube reinforced polyimide composites. *Compos. Sci. Technol.*, **63**(11):1637-1646. http://dx.doi.org/10.1016/S0266-3538(03)00067-8

Srivastava, N., Banarjee, K., 2005. Performance analysis of carbon nanotube interconnects for VLSI applications. IEEE/ACM Int. Conf. Computer-Aided Design, p.383-390. http://dx.doi.org/10.1109/ICCAD.2005.1560098

Srivastava, N., Li, H., Kreupl, F., *et al.*, 2009. On the applicability of single-walled carbon nanotubes as VLSI interconnects. *IEEE Trans. Nanotechnol.*, **8**(4):542-559. http://dx.doi.org/10.1109/TNANO.2009.2013945

Thess, A., Lee, R., Nikolaev, P., *et al.*, 1996. Crystalline ropes of metallic carbon nanotubes. *Science*, **273**(5274):483-487. http://dx.doi.org/10.1126/science.273.5274.483

Yuzvinsky, T.D., Mickelson, W., Aloni, S., *et al.*, 2006. Shrinking a carbon nanotube. *Nano Lett.*, **6**(12):2718-2722. http://dx.doi.org/10.1021/nl061671j

Zhao, Y.P., Wei, B.Q., Ajayan, P.M., *et al.*, 2001. Frequency-dependent electrical transport in carbon nanotubes. *Phys. Rev. B*, **64**(20):201402. http://dx.doi.org/10.1103/PhysRevB.64.201402

Zhou, Y., Sreekala, S., Ajayan, P.M., *et al.*, 2008. Resistance of copper nanowires and comparison with carbon nano-tube bundles for interconnect applications using first principles calculations. *J. Phys.-Condens. Matter*, **20**(9):1-5. http://dx.doi.org/10.1088/0953-8984/20/9/095209